

J. KUSIŃSKI\*<sup>#</sup>, A. KOPIA\*, Ł. CIENIEK\*, S. KAĆ\*, A. RADZISZEWSKA\*

**DEPOSITION OF OXIDE AND INTERMETALLIC THIN FILMS BY PULSED LASER (PLD)  
AND ELECTRON BEAM (PED) METHODS**

**OSADZANIE TLENKOWYCH ORAZ MIĘDZYMETALICZNYCH CIENKICH FILMÓW Z WYKORZYSTANIEM  
LASERA IMPULSOWEGO (PLD) I WIĄZKI ELEKTRONOWEJ (PED)**

In this work the pulsed laser deposition (PLD) and the pulsed electron beam deposition (PED) techniques were used for fabrication of Mo-Bi<sub>2</sub>O<sub>3</sub>, La<sub>1-x</sub>Sr<sub>x</sub>CoO<sub>3</sub>, La<sub>1-x</sub>Ca<sub>x</sub>CoO<sub>3</sub> and Al-Mg thin films. An influence of ablation process basic parameters on the coatings structure and properties was discussed. Two types of laser ablation systems were applied: one equipped with a KrF excimer and second with a Q-switched Nd:YAG. Films were deposited on Si and MgO substrates. Scanning (SEM) and transmission (TEM) electron microscopy, atomic force microscopy (AFM) as well as X-ray diffraction (XRD) were used for structural analysis. Investigations focused on structure and chemical composition showed that smooth and dense thin films with nanocrystalline structure, preserving the composition of the bulk target, could be obtained by the both PLD and PED techniques. Research study showed that by a proper selection of PLD and PED process parameters it was possible to deposit films with significantly decreased amount and size of undesirably nanoparticles.

*Keywords:* PLD, PED, thin films, structure, doped oxides

Osadzanie laserem impulsowym (PLD) oraz osadzanie impulsową wiązką elektronową (PED) wykorzystane zostało do wytwarzania cienkich filmów typu: Mo-Bi<sub>2</sub>O<sub>3</sub>, La<sub>1-x</sub>Sr<sub>x</sub>CoO<sub>3</sub>, La<sub>1-x</sub>Ca<sub>x</sub>CoO<sub>3</sub> oraz Al-Mg. Dyskutowano wpływ podstawowych parametrów procesu ablacji na strukturę i właściwości uzyskiwanych powłok. Wykorzystane zostały dwa typy systemów do ablacji; jeden z ekscymerowym laserem KrF i drugi na bazie lasera Nd:YAG z modulatorem dobroci (Q-Switch). Filmy osadzano na podłożu Si i MgO. Skaningowa (SEM) i transmisyjna (TEM) mikroskopia elektronowa, mikroskopia sił atomowych (AFM), oraz dyfrakcja rentgenowska (XRD) wykorzystana została do analizy strukturalnej. Badania skoncentrowane na strukturze i składzie chemicznym wykazały jednorodną i zwartą budowę cienkich nanokrystalicznych filmów uzyskanych metodami PLD i PED utrzymujących skład odparowywanych tarcz. Wykazano doświadczalnie, że odpowiednie dobranie parametrów procesu pozwala otrzymywać filmy o istotnym zminimalizowaniu ilości i wymiarów niekorzystnych nanocząstek w powłoce.

## 1. Introduction

During the past 30 years a rapid progress in the range of surface engineering techniques, which are available to modify the material surfaces, is observed. Recent developments of the thin film deposition technologies permitted not only to expand application of the conventional – chemical vapor deposition (CVD) and physical vapor deposition (PVD) methods, but also to find new ways of getting highly energetic, activated vapor (in a form of a flux of highly energetic atoms, ions or clusters) [1-3]. Indeed, due to a high mean energy of activated vapor, several orders of magnitude greater than that obtained in conventional

processes, it is possible deposition, at relatively low temperature, layers and multilayers, composed of single or multi elements (metals and other materials) that are extremely thin and characterized by a very good adhesion to the substrate [3]. Such thin films and coatings, known as functional, are used to modify the optical characteristics of the material surfaces (the substrate), their electrical conductivity, and hardness or lubricity, as well as to provide corrosion resistance, chemical activity or inertness, or simply for decoration [1-5].

Nowadays, there are many kinds, versions and modifications of PVD techniques [2,3]. Application of two advanced deposition techniques (namely PLD and PED), that use material

\* AGH-THE UNIVERSITY OF SCIENCES AND TECHNOLOGY, AL. A. MICKIEWICZA 30, 30-059 KRAKOW, POLAND

# Corresponding author: kusinski@agh.edu.pl

ablation and vapor deposition for producing high quality thin films of dielectric inorganic- and organic compounds and alloys, is presented in this paper.

The PLD technique – *pulsed laser deposition* has been applied in 80-thies and is still under expansion for practical applications [4-6]. As shown in our previous paper [7] in case of the PLD technique, the target material is placed inside a chamber with a controlled atmosphere (vacuum or reactive gas) where is irradiated, through an optical window by a high fluency, focused, laser beam. Usually, a vacuum chamber is equipped with a rotating target support and a substrate holder, which can be resistively heated up to 900°C. The PLD is a complex physical process in which several phenomena occur [8]. During early stages of the ablation process several subsequent processes, like: photon energy absorption, rapid heating and melting, vaporization and vapor ionization, plasma emission, plasma heating, as well as detonative plasma expansion, take place due to interaction of the laser beam with the target surface. In general, the thin film deposition process, involves evaporation of material (being in the form of a solid target) by pulsed laser beam of very short duration (from micro- to nano- and even femtoseconds) focused on the material surface (target) and of very high fluence and then vapor deposition and thin film growth on the substrate. The dominant mechanisms involved in the formation of a hot plasma from the irradiated surface were found to depend sensitively on laser parameters such as the energy density (fluence), pulse duration, wavelength, polarization, laser repetition rate, as well as the properties of irradiated material [4-8]. The laser's temporal pulse length can have a significant effect on the dynamics of the ablation process. In general, as the pulse length is shortened, energy is more rapidly transferred into the material leading to a more rapid material ejection. With a laser beam of a short wavelength (high photon energy), the photo-thermal mechanisms for ablation are active (direct bond-breaking, and explosive disintegration of the material lattice), indeed rather sublimation of material (being in solid state form) than its evaporation from the liquid phase occurs [8-10]. With higher fluence and longer wavelength (lower photon energy) melting, boiling and vaporization process take place (frequently explosive boiling happens) [8-10]. The vapor plume formed during laser beam-target interaction expands perpendicularly away from the target and condenses on a substrate, placed at a certain distance from the target. The thin film grows with a rate reaching of a few dozens of nanometer/pulse. The PLD is probably one of the simplest techniques for thin films manufacture [4,9,11]. Vapor cloud emitted from the target material during ablation process shows many singularities, different from these of vapors formed in other PVD techniques [4]. Actually, it is well experienced that the PLD has a unique capability to produce high-quality thin films of various kinds of materials [12,13]. The technique is also frequently used in elaboration of thin films used as gas sensors and catalytic devices, multilayer coatings for tribological, medical and anticorrosive applications [14-17], as well as, thin films for microelectronics (thin films of superconductors and piezoelectrics) [12,13,18].

A similar to the PLD growth method, based on the use of a pulsed energy beam to ablate a target material and to form a plasma plume, was developed more recently: the *pulsed electron beam deposition* (PED) [19-21]. The concept of these techniques, is similar to the PLD but the PED is based on much simpler equipment and is a relatively new method applied for thin film deposition. The main difference between PED and PLD methods is that the absorption of the electron energy by the target material is not limited and is not dependent on the optical properties of the material (surface reflectivity), as in the case of the PLD [20]. In case of the PED the target evaporation is governed by electrons, not by photons, and thus the energy transfer into the target surface is more effective than in the PLD. During the PED process, the electron beam energy is absorbed within a very thin subsurface layer of a target leading to extremely rapid heating and evaporation of the material and formation of plasma having the shape of a plume. Moreover, contrary to the laser beam, which is screened by the vapor cloud, the majority of the electron energy is absorbed, hence vapor gets ionized, and becomes a plasma plume. In both cases, expansion of the dense plasma in the direction perpendicular to the surface is seen as a plasma plume. Potential advantages of pulsed electron beam sources, in comparison with lasers with similar power densities ( $10^8 \text{ Wcm}^{-2}$ ), include higher electrical efficiency (up to 30% in the case of a channel-spark discharge), the ability to process materials that are transparent (characterized by a wide band gap) or highly reflective to laser light and lower capital costs [21,22]. Compared with the laser ablation, the pulsed intense electron beam has optimum parameters for ablation in a very narrow gas pressure range from 0,007 to 0,02 mbar. This limited pressure range is, however, suitable for growing thin films of complex oxides with different physical properties. Since the first report [19] concerning deposition of superconducting YBaCuO thin films by pseudo spark ablation the PED was used to grow thin films of oxide materials such as high temperature superconductors [20, 23], hydroxyapatite, bio-active glasses, organic materials [20], colossal magneto-resistance materials [24],  $\text{SnO}_2$  [25], zirconium tin titanate [26] and ZnO [27].

In this paper, we report our recent experimental results on application of the PLD and PED methods for the ablation of material from a solid target and the deposition of functional multi-component thin films. In this studies, Al-Mg alloy and oxide materials:  $\text{Bi}_2\text{O}_3 + 15\% \text{ wt. Mo}$ ,  $\text{La}_{1-x}\text{Sr}_x\text{CoO}_3$ ,  $\text{La}_{1-x}\text{Ca}_x\text{CoO}_3$ , were used as targets. The surface morphology, microstructure and composition of the grown films were studied in close correlation with the characterizations of parameters determining the optimum growth conditions.

## 2. Experimental

The thin films discussed in this paper were grown at AGH Krakow using, the Neocera Pioneer equipped with PLD and PED systems. Fig. 1 shows the Neocera Pioneer equipped with the PLD and PED systems and the PED experimental set-up (Fig. 1b)

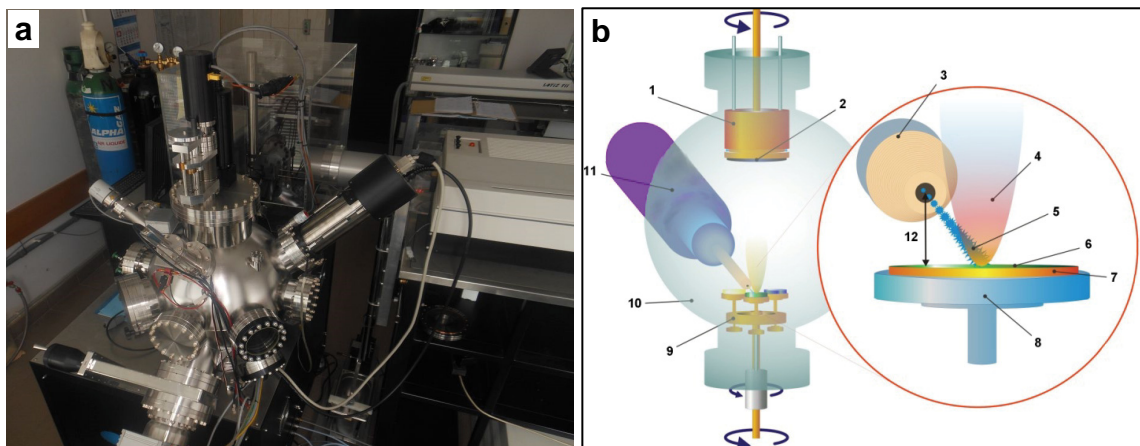


Fig. 1. The Neocera Pioneer equipped with PLD and PED systems – (a) and the PED experimental set-up (b): 1 – rotating substrate heater; 2 – substrate; 3 – flange to vacuum system with glass tube; 4 – plasma plume; 5 – electron beam; 6 – target; 7 – cooper bias; 8 – rotating target; 9 – rotating targets carousel; 10 – vacuum chamber (anode); 11 – pulsed electron source; 12 – distance between the capillary tube and the target

installed at AGH. For the PLD process a Q-switched Nd-YAG laser, with a wavelengths  $\lambda = 266$  nm and  $\lambda = 1064$  nm, a laser fluence  $q = 3.5$  J/cm<sup>2</sup> and  $q = 8.2$  J/cm<sup>2</sup>, was used. For the PED process a pulsed electron source (PEBS-20), with an accelerating voltage  $U = 8$ -20 kV, pulse width =  $\sim 100$  ns, single pulse energy = 0,1-0,8 J, pulse energy density = 13 J/cm<sup>2</sup> and pulse repetition rate = 15Hz, was applied. Some films were produced at Krakow Academic Center for Materials and Nanotechnology (ACMIN) using, the Neocera Pioneer equipped with a Coherent COMPexPro 110F KrF ( $\lambda = 248$  nm) excimer laser generating beam of photons with pulses of 10 ns duration, frequency  $f = 10$  Hz and fluence  $q = 2$  J/cm<sup>2</sup>.

The surface morphology of the deposited films was examined using an AFM – Veeco DIMENSION ICON-PT and SEM – FEI Inspect S50. Microstructure of the thin films was characterized by using SEM – FEI Nova NanoSEM 450 and TEM – JEOL JEM-2010 ARP. TEM investigations were carried out on cross-sectional thin foils prepared by the precision ion polishing system (PIPS). Chemical composition was investigated by an energy dispersive X-ray spectroscopy (SEM-EDS, TEM-EDS and STEM-EDS). Phase identification was performed using selected area electron diffraction (SAED) and X-ray diffraction (XRD) techniques. The SAED patterns were interpreted using the Java Electron Microscopy software (JEMS) [28]. The crystalline structure of thin films was examined by means of the X-ray analysis (PANanalytical EMPYREAN DY 1061) with Cu  $K_{\alpha}$  radiation in Bragg-Brentano and grazing geometry  $\alpha = 1^{\circ}$ .

### 3. Results and discussion

In this section, results of the surface morphology, microstructure and the composition examinations of the films of oxide materials: Bi<sub>2</sub>O<sub>3</sub> + 15% wt. Mo, La<sub>1-x</sub>Sr<sub>x</sub>CoO<sub>3</sub>, La<sub>1-x</sub>Ca<sub>x</sub>CoO<sub>3</sub> and Al-Mg alloy, grown by using the pulsed energy beam deposition methods (PLD and PED), are presented and discussed.

#### 3.1. PLD deposition of the bismuth oxide

Bismuth oxides are well-known as good ion conducting solid electrolytes [29]. The phase  $\alpha$ -Bi<sub>2</sub>O<sub>3</sub> with the FCC fluorite-type structure which is stable over a narrow temperature range, 729-825°C is one of the best oxide ionic conductor, however, below 729°C, it transforms into series of phases with lower ionic conductivity [29, 30]. Bismuth oxides present also important optical and electrical applications. Sakai et al. [31] studied a wide range of oxides for NO / NO<sub>2</sub> distinction. They propose the Bi<sub>2</sub>O<sub>3</sub> as a highly selective oxide for NO detection. It had been earlier also used for the smoke detection [32]. The most widely used method for stabilization of  $\alpha$ -Bi<sub>2</sub>O<sub>3</sub> (in term to get the defect structure of fluorite-type and high ionic conductivity at low temperature range) consists of doping with Mo, Y, V, Cu, Nb and Er atoms [33,34]. The aim of this research was to produce and characterize the Mo-doped Bi<sub>2</sub>O<sub>3</sub> thin films deposited by PLD technique on the monocrystalline Si substrate. Dense nanocrystallized Mo-doped Bi<sub>2</sub>O<sub>3</sub> films were prepared, in an oxygen atmosphere, by material evaporation from the compacted and sintered targets. The deposition was carried out at 600°C for 15 - 30 min, using the Neocera Pioneer PLD system equipped with a Q-switched Nd-YAG laser, with a wavelength  $\lambda = 266$  nm and a laser fluence  $q = 3.5$  J/cm<sup>2</sup>. SEM and TEM were employed to characterize the PLD deposited Mo-Bi<sub>2</sub>O<sub>3</sub> thin films microstructure. Depending on the deposition time, the film thickness varied from 130 to 500 nm. SEM images of the deposited film are presented in (Fig. 2). SEM investigations showed that under deposition conditions the Mo-doped Bi<sub>2</sub>O<sub>3</sub> film surface is smooth, however, some droplets with an average size  $< 1$   $\mu$ m of target material are also present on the film surfaces. The surface roughness increases for thicker films (500 nm), what can be beneficial when using them as the gas sensors.

The bright-field TEM image showing microstructure of the deposited 500 nm film is presented in (Fig. 3).

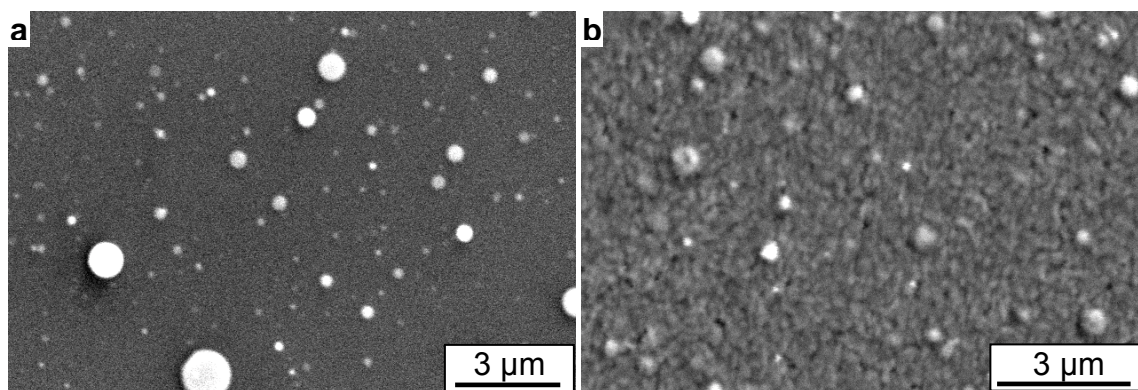


Fig. 2. SEM images show the surface morphology of the  $\text{Bi}_2\text{O}_3 - \text{Mo}$  15 wt% thin films grown at  $T_s = 600^\circ\text{C}$  at  $T_p = 25^\circ\text{C}$  using Q-switched Nd-YAG laser ( $\lambda = 266 \text{ nm}$ ) with the fluence of  $q = 3,5 \text{ J/cm}^2$  for different deposition time; different film thickness: a – 130 nm and b – 500 nm

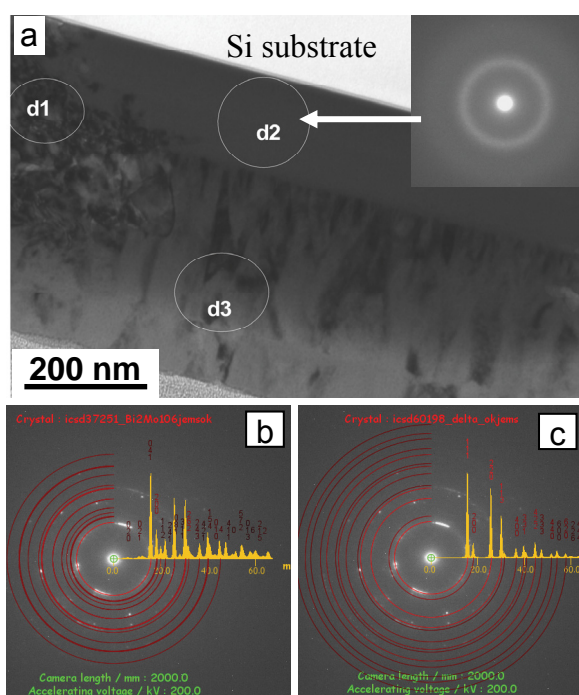


Fig. 3. TEM cross-section thin foil showing microstructure of the 15 wt% Mo doped bismuth oxide film (a) and SEAD patterns taken from the areas marked as 2d and 3d on (a) and their identification.

Due to the presence of oxygen during the ablation process, an amorphous film of  $\text{SiO}_2$  was formed between the Si substrate and  $\text{Mo-Bi}_2\text{O}_3$  thin film. Undoubtedly, the presence of the amorphous  $\text{SiO}_2$  layer is probably the reason of creating amorphous structure of the near substrate layer in the doped bismuth oxide thin film (as revealed by diffraction pattern – inset in (Fig. 3a)). The amorphous layer is not continuous. In some areas the thin film grows as the crystalline film directly on the amorphous  $\text{SiO}_2$  layer. The middle and top layers of the film were characterized by a columnar nanometric structure. Phase identification by electron diffraction revealed presence of  $\text{Bi}_{26}\text{Mo}_{10}\text{O}_{69}$ ,  $\text{Bi}_2\text{Mo}_1\text{O}_6$ ,  $\text{Bi}_{3.2}\text{Mo}_{0.8}\text{O}_{7.5}$  and  $\text{d-Bi}_2\text{O}_3$  phases (Fig. 3b,c). STEM-EDS analysis confirmed the presence of Bi, Mo and O in the film, however, their distribution is not homogenous and the Mo / Bi ratio changes in the film thickness [35].

### 3.2. PLD and PED deposition of perovskite oxides

Perovskite oxides ( $\text{ABO}_3$ ) are used as gas sensor materials due to their thermal stability at different atmospheres. Microstructure and chemical composition – concentration of acceptor/donor dopant atoms, can influence significantly values of the resistance and conductivity changes of  $\text{ABO}_3$  oxides with temperature. Substitution of  $\text{Sr}^{2+}$  or  $\text{Ca}^{2+}$  ions for  $\text{La}^{3+}$  ion in  $\text{LaCoO}_3$  results in considerable change of its magnetic and electric properties. Doping with strontium ions is aimed at increasing the conductivity of cobaltite. This effect is acquired by doping up to 50 at.% of Sr and temperature-governed modulation [35]. For catalytic applications the  $\text{LaCoO}_3$  perovskite doped by different elements is mainly used in a form of powders [36-38]. The research already carried out by Yang et al. [37] showed that CO undergoes total oxidation into  $\text{CO}_2$  at temperature of  $260^\circ\text{C}$ . The powders obtained by the authors were characterized by large-sized grains (120 nm).  $\text{La}_{1-x}\text{Sr}_x\text{CoO}_3$  compounds in the form of thin layers are produced by the laser ablation method or by chemical methods and they are used as electrodes in fuel cells or gas sensors [39-42]. In our previous investigations [12,43], optimal conditions for the production of nanocrystalline thin films of  $\text{LaCoO}_3$  doped with Sr by laser ablation method using the Nd-YAG and excimer lasers were found. The results of the investigation of influence of Sr and Ca additions on the structure of the  $\text{La}_{1-x}\text{Sr}_x\text{CoO}_3$  and  $\text{La}_{1-x}\text{Ca}_x\text{CoO}_3$  thin films deposited using excimer laser and PED technique are present in this section. The  $\text{La}_{1-x}\text{Sr}_x\text{CoO}_3$  targets were purchased from Lesker Company. The  $\text{La}_{1-x}\text{Sr}_x\text{CoO}_3$  ( $x = 0, 0.1, 0.2$ ) thin films were deposited on [100] oriented Si substrates heated up to  $600^\circ\text{C}$ , using the Neocera Pioneer PLD system equipped with the Coherent COMPexPro 110F KrF ( $\lambda = 248 \text{ nm}$ ) excimer laser generating photon pulsed beam of 10 ns duration, frequency  $f = 10 \text{ Hz}$  and fluence  $q = 2 \text{ J/cm}^2$ . The other parameters of the deposition process were following: a target-substrate distance of 80 mm, the oxygen pressure in the deposition chamber was  $p = 13 \text{ Pa}$ . SEM images in the (Fig. 4) show the surface morphology of the  $\text{La}_{1-x}\text{Sr}_x\text{CoO}_3$  thin films (with  $x = 0$  and 0.1).

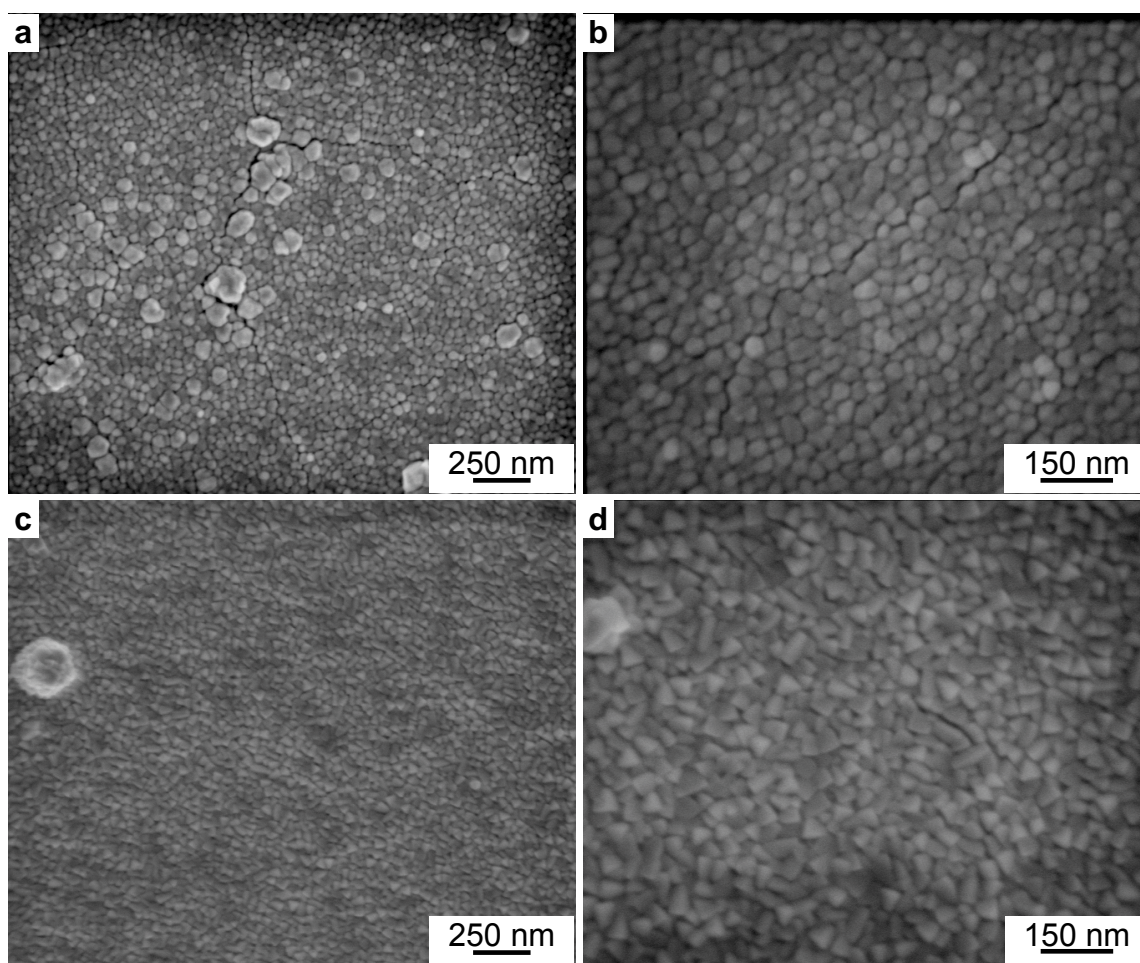


Fig. 4. SEM images show the surface morphology of the  $\text{LaCoO}_3$  – (a, b) and  $\text{La}_{0.9}\text{Sr}_{0.1}\text{CoO}_3$  – (c, d) deposited using, the Coherent COMPexPro 110F KrF ( $\lambda = 248$  nm) excimer laser pulses of 10 ns duration, frequency  $f = 10$  Hz and fluence  $q = 2$  J/cm<sup>2</sup>

The deposited films are practically free of droplets. Surface examinations revealed that the grain size of Sr-doped  $\text{LaCoO}_3$  films was smaller than the grain size of the undoped  $\text{LaCoO}_3$ . Moreover, doping with Sr atoms not only changed the grain size in the thin film but also changed their shape. The undoped layers had the shape of polygons with the grain size of 49 nm (Fig. 4a, b). As a result of Sr-doping, the grain shape changed to the triangular shape with a size of 32 nm (Fig. 4c-d). Change of the grain's shape as well as of preferred orientation of growth as a result of doping in the film deposited by PLD method was also observed in case of  $\text{CeO}_2$  thin films doped by Nd [44]. Results of X-ray diffraction analysis of  $\text{La}_{1-x}\text{Sr}_x\text{CoO}_3$  thin films can be seen in (Fig. 5). Identification of phases was based on the JCPDS base card numbers 04-007-6831 ( $\text{LaCoO}_3$ ), 00-028-1229 ( $\text{La}_{0.9}\text{Sr}_{0.1}\text{CoO}_3$ ) and 04-007-8983 ( $\text{La}_{0.8}\text{Sr}_{0.2}\text{CoO}_3$ ). The study showed that the PLD process parameters were set correctly and it was possible to obtain polycrystalline layers of the assumed phase composition and of the rhombohedral structure. The deposited  $\text{La}_{1-x}\text{Sr}_x\text{CoO}_3$  films were textured, strongly oriented in the [100] direction. On the basis of the results determined from the Williamson-Hall plot, the average crystallite size for each layer was calculated. Results are summarized in (Table 1).

TABLE 1

The crystalline size and grain size of  $\text{La}_{1-x}\text{Sr}_x\text{O}_3$  ( $x = 0, 0.1, 0.2$ ) thin films

Composition	Crystalline size W-H [nm]	Grain size SEM [nm]
$\text{LaCoO}_3$	52	49
$\text{La}_{0.9}\text{Sr}_{0.1}\text{O}_3$	29	32
$\text{La}_{0.8}\text{Sr}_{0.2}\text{O}_3$	30	33

The results reported in (TABLE 1) revealed that the crystallites in Sr-doped layers were smaller than in the undoped layers. A similar effect was observed by Sun [44] and by Lv [46] as a result of  $\text{LaCoO}_3$  doping with Mg. Decrease of the grain size could be explained by migration of dopant into the grain boundaries and thus the introduction of the crystal lattice disorder, resulting in a reduction in crystallite size [46]. Comparison of the diffraction patterns for the undoped and doped layers (Fig. 5) showed the small displacement the diffraction lines (individual peaks) towards higher values of  $2\theta$ . This could be due to the fact that La has smaller atomic radius (195 pm) than Sr (200 pm) which may cause a slight deformation of the unit cell. Small changes of the lattice parameter with doping level were also observed by Kumar et al. [47].

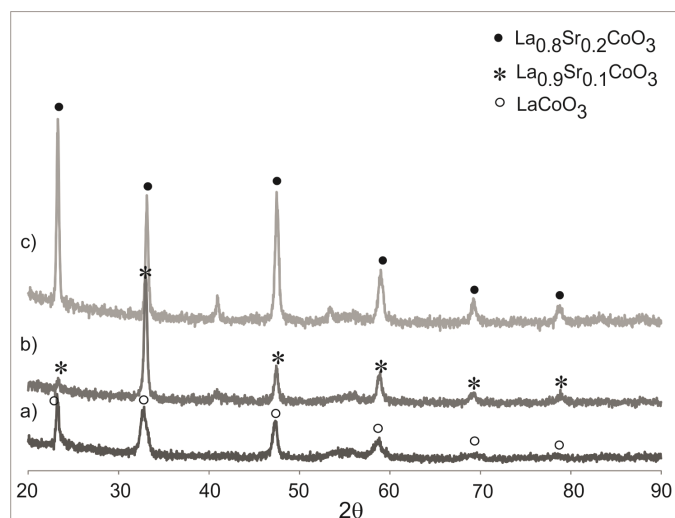


Fig. 5. X-ray diffraction spectrums recorded in grazing geometry  $\alpha = 1^\circ$ , from the thin films of a)  $\text{LaCoO}_3$ , b)  $\text{La}_{0.9}\text{Sr}_{0.1}\text{CoO}_3$ , c)  $\text{La}_{0.8}\text{Sr}_{0.2}\text{CoO}_3$  by PLD method

Thin films of  $\text{La}_{1-x}\text{Ca}_x\text{CoO}_3$  were deposited by the PLD and the PED on the  $\text{MgO}$  substrates. The experiments revealed

a strong effect of the deposition parameters on the structural characteristics of  $\text{LaCaCoO}_3$  thin films. A representative results of the surface morphology of the grown  $\text{LaCaCoO}_3$  thin films with using the optimized conditions for the PLD and the PED processes are presented in Figure 6 by SEM (Fig. 6a, b) and AFM (Fig. 6c, d) images, respectively.

These examinations revealed that the grain size of PED deposited films was smaller than the grain size of films deposited by PLD technique. Examinations using the cross-sectional TEM analysis in thin film micro areas indicated that the average grain size of PLD deposited  $\text{LaCaCoO}_3$  thin films was about 20-40 nm and was finer than that observed for PED (30-60 nm, see (Figs. 7, 8).

However, the SEAD ring patterns recorded in thin films produced by PED (see inset in (Fig. 8a, e) could suggest that a finer grain structure was obtained than that for PLD. Probably, the ring SEAD pattern was resulted from nanometric grain substructure for PED deposited  $\text{LaCaCoO}_3$  films. From the selected area diffraction pattern (SAED) in (Fig. 7b), one could conclude that the  $\text{LaCaCoO}_3$  films deposited by PLD on  $\text{MgO}(100)$  might grow epitaxially. It was not so evident in case of PED deposition.

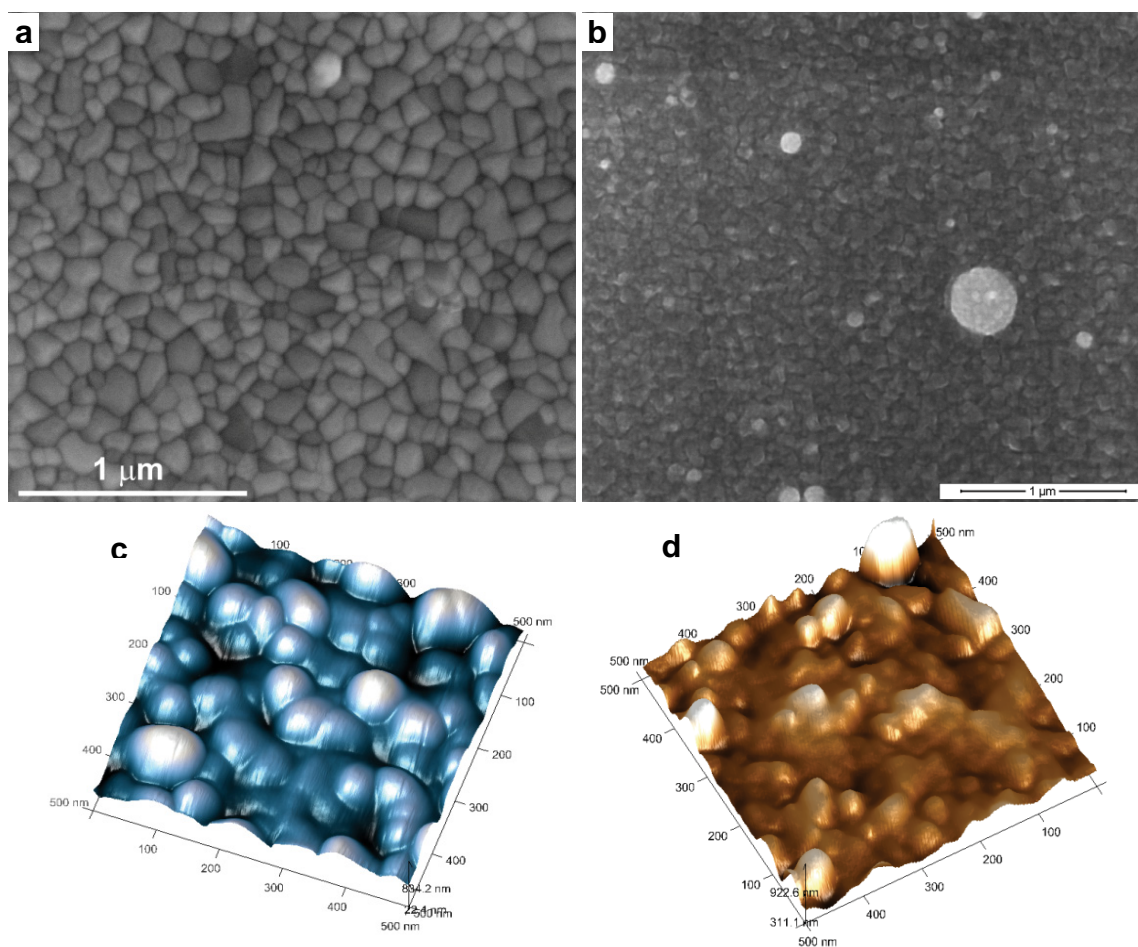


Fig. 6. SEM and AFM surface morphology images for  $\text{LaCaCoO}_3$  perovskite thin films deposited by PLD (a, c) and PED (b, d) techniques

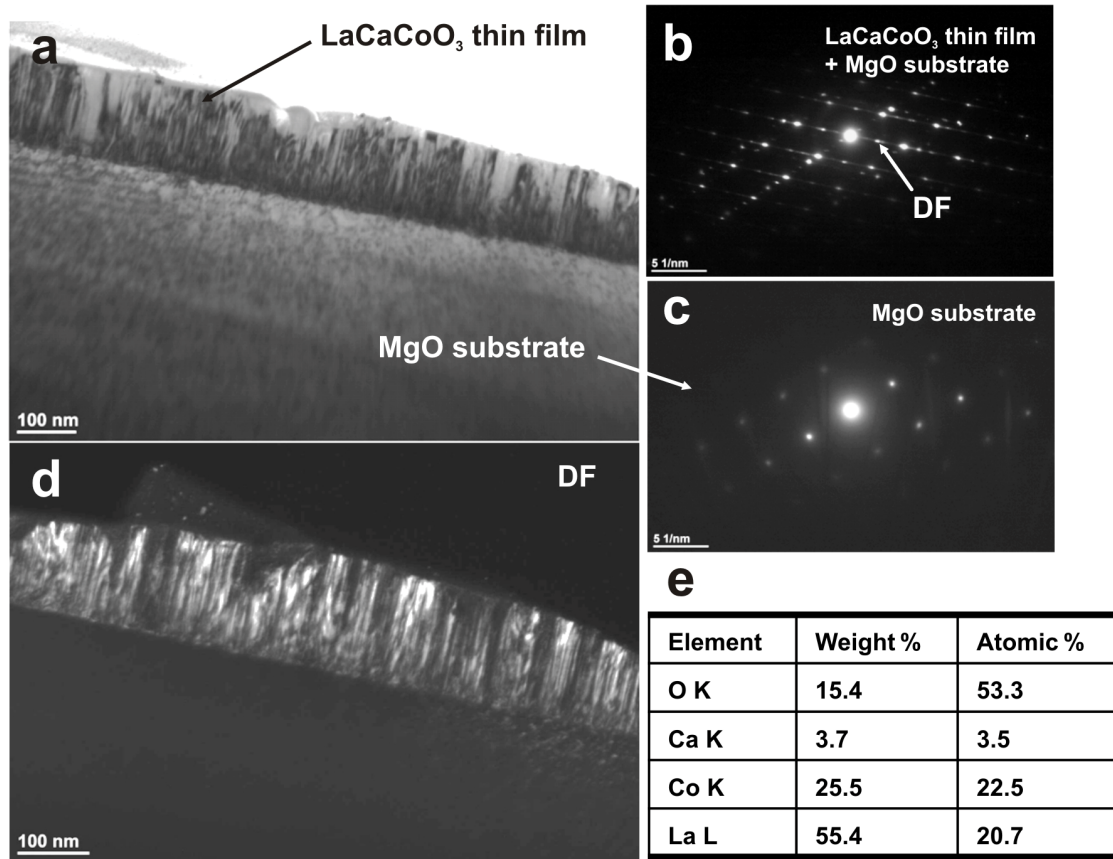


Fig. 7. TEM cross-section bright and dark field images (a, d), diffraction patterns (b, c) with EDS chemical composition results for the LaCaCoO<sub>3</sub> perovskite thin film deposited by PLD on the MgO substrate

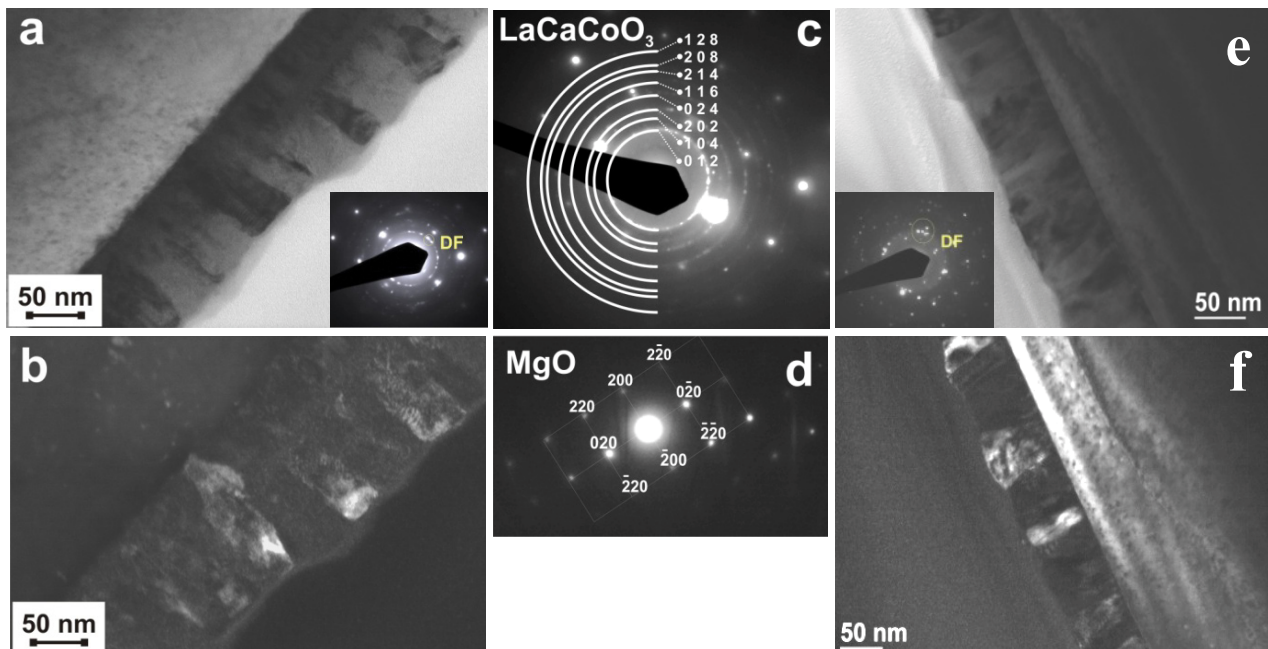


Fig. 8. TEM cross-section bright and dark field images for LaCaCoO<sub>3</sub> perovskite thin films deposited by PED on the MgO substrate with different electron energy (a, b – 12 kV; e, f – 10 kV); diffraction patterns solved for the thin film and the substrate (c, d)

### 3.3. PLD deposition of Al-Mg alloys

Al-Mg alloys are applied in various industries as the lightest materials, because of their desirable features, e.g. low mass density and better corrosion resistance when they cover magnesium and its alloys, especially. Cubic  $\beta$ - $\text{Al}_3\text{Mg}_2$  phase is a very attractive material of a great interest for aeronautics. Laser ablation process is the most novel technique used for production of  $\beta$ - $\text{Al}_3\text{Mg}_2$  thin films [48]. In our laboratory, Radziszewska used recently successfully this technique for production of  $\beta$ - $\text{Al}_3\text{Mg}_2$  thin films [49,50]. The Al-Mg films, discussed in this chapter, were grown by the pulsed laser deposition technique using a QS-Nd:YAG laser. The deposition process involved the use of a target

with the nominal composition of 60.9 at.% Al and 39.1 at.% Mg. Deposition was carried out at 25°C, using the Neocera Pioneer PLD system equipped with a Q-switched Nd-YAG laser, with a wavelength  $\lambda = 1064$  nm, pulse duration of 18 ns, 10 Hz repetition rate and laser fluence  $q = 8.2$  J/cm<sup>2</sup>. Figure 9 shows the TEM bright- and dark-field images and SEAD patterns recorded in the marked areas of Al-Mg thin film. This film was composed of three layers with different structure. The first one, growing directly onto the Si substrate, was characterized by ultrafine crystalline structure near the Si substrate (with the crystal size  $\sim 5$ -20 nm) which gradually changed to an amorphous structure (as indicated by dark-field image in (Fig. 9b) and SEAD ring pattern (Fig. 9c). The thickness of this layer reached 80-100 nm (Fig. 9a).

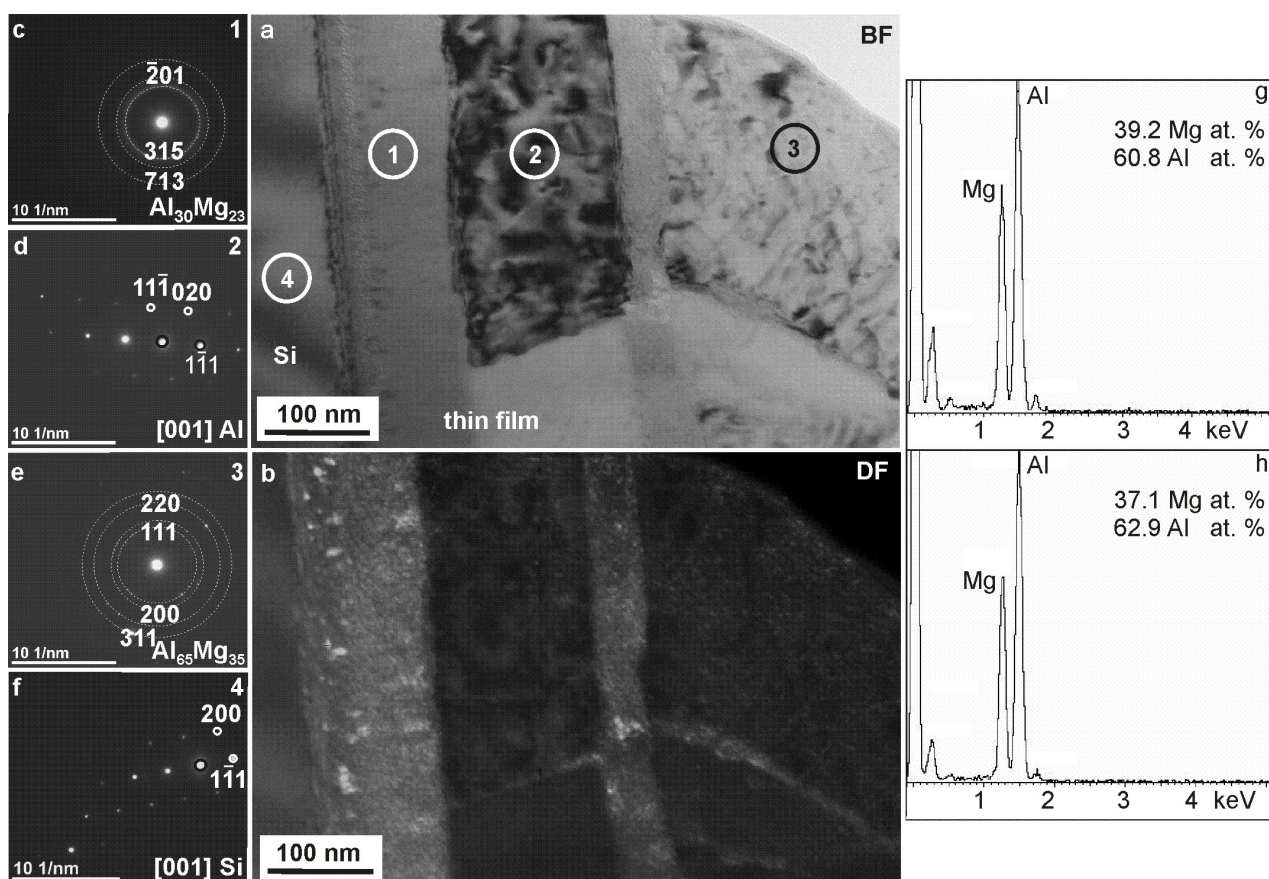


Fig. 9. TEM bright- (a) and dark-field (b) images of the Al-Mg thin film deposited at  $T_p = 25^\circ\text{C}$  using Q-switched Nd-YAG laser ( $\lambda = 1064$  nm) with the fluence of  $13.6$  J/cm<sup>2</sup>; (c-f), SEAD patterns recorded in the marked in (a) areas (1-4) of the film cross-section and EDS chemical analysis in thin film layer near the Si substrate (g), and in the surface layer (h)

The electron diffraction analysis indicated presence of  $\text{Al}_{30}\text{Mg}_{23}$  tetragonal phase. The next layer, middle layer, was identified by SEAD analysis as Al one (Fig. 9d). A nanocrystalline FCC structure of  $\text{Al}_{65}\text{Mg}_{35}$  phase was observed in the top layer of the film. Similar morphology of the Al-Mg thin films was observed with using other PLD conditions [49,50]. EDS chemical analysis (Figs. 9g, h) revealed that the thin film layer near the Si substrate contained 39.2 Mg at.%, 60.8 Al at.% (Fig. 9g) which was very close to the target composition (39.1 Mg at.%, 60.9 Al at.%), while chemical composition of

the surface layer was richer in Al, containing: 62.9 Al at.% and 37.1 Mg at.% (Fig. 9h).

### 4. Concluding remarks

Examples of thin films deposited by the PLD and PED methods, were presented in this paper. They were selective and represent only small part of research work carried out at the Department of Surface Engineering and Materials Characteriza-

tion AGH. For all the oxide compounds studied in this work, we never observed the presence of the undesirably micrometric size droplets which are present on the surface of films grown by the PLD and specially by PED. In addition, the composition of the various oxide thin films investigated in this work was close to that of the target, even in the case of the complex oxide compounds. Hence, smooth and dense thin films preserving the composition of the bulk target could be obtained by the PED method, thus the PED appears was very promising for thin film growth, even in competition with the pulsed laser deposition (PLD).

#### Acknowledgements

This work was carried out within a project No 11.11.110.936. The authors are grateful to Prof. Boguslaw Major, one of the first scientists in Poland having enthusiasm for study of the pulsed laser deposition. He allowed us to see that the enjoyment of the PLD method could be focused at the exploration and evolution of this technique as well as the development of a new ones. We are grateful to Prof. Boguslaw Major for inviting us to present our paper in this special issue.

#### REFERENCES

- [1] D.S. Rickerby, A. Matthews, *Advanced Surface Coatings: a Handbook of Surface Engineering*, Chapman and Hall, New York, 1991.
- [2] T. Burakowski, T. Wierzchon, *Surface engineering of metals: principles, equipment, technologies*, CRC Press, 1999.
- [3] B.G. Wendler. *Functional coatings by PVD or CVD Methods*, ITE Radom, ISBN 978-83-7789-001-1, 2011.
- [4] J.M. Lackner, *Industrially-scaled hybrid Pulsed Laser deposition at room temperature*, OREKO sc., Krakow 2005.
- [5] B. Major, *Ablacja i osadzanie laserem impulsowym*, Akapit, Kraków, 2002.
- [6] C. Belouet, *Appl. Surf. Sci.* **96-98**, 630-642 (1996).
- [7] J. Kusiński, S. Kaç, A. Kopia, A. Radziszewska, M. Rozmus-Górniakowska, B. Major, Ł. Major, J. Marczak, A. Lisiecki, *Bulletin of the Polish Academy of Sciences. Technical Sciences* **60**, 4, 711-728 (2012).
- [8] J. Marczak, *Analiza i usuwanie nawarstwień obcych z różnych materiałów metodą ablacji laserowej*, BEL studio Sp. z o.o., Warszawa, 2004.
- [9] A.A. Voevodin, S.J.P. Laube, S.D. Walck, J.S. Solomon, M.S. Donnelly, J.S. Zabinski, *Combined of magnetron sputtering and pulsed laser deposition of carbides and diamond-like films*, *Journal of Applied Physics* **78**, 4123 (1995).
- [10] H.U. Krebs, S. Fühler and O. Bremert, *Applied Surface Science* **86**, 86-89 (1995).
- [11] B. Major, F. Bruckert, J.M. Lackner, R. Ebner, R. Kustos, P. Lacki, *Arch. Metal. and Mater.* **53**, 39-48 (2008).
- [12] D.B. Chrisey, G.K. Hubler (Eds.), *Pulsed Laser Deposition of Thin Films*, John Wiley & Sons, New York, 1994.
- [13] L. Cieniek, J. Kusinski, *Inżynieria Materiałowa* **4**, 253-256 (2013).
- [14] B. Major, *Archives of Metallurgy and Materials* **50**, 35-46 (2005).
- [15] L. Major, J. Morgiel, J.M. Lackner, M. Kot, M. Szczerba, B. Major, *Advances Engineering Materials*, Viley-VCH **7**, 617-621(2008).
- [16] B.Major, F.Bruckert, J.M.Lackner, R.Ebner, R.Kustos, P.Lacki, *Arch. Metal. and Mater.* **53**, 39-48 (2008).
- [17] L.Major, J.M.Lackner, M.Kot, M.Janusz, B. Major, *Bull. Pol. Ac Tech.* **62**, 3 565-570 (2014).
- [18] A. Kopia, *Materiały półprzewodnikowe o właściwościach katalitycznych*, Wydawnictwo AGH, Kraków, 2011.
- [19] M. Hobel, J. Greek, G. Linker, C. Schultheiss **56**, 10, 973-975 (1990).
- [20] R.J. Choudhary, S.B. Ogale, S.R. Shinde, V.N. Kulkarni, T. Venkatesan, K. S. Harshavardhan, M. Strikovski, B. Hannover, *Appl. Phys. Lett.* **84** 1483 (2004).
- [21] G. Müller, M. Konijnenberg, G. Krafft, C. Schultheiss, *Deposition by means of pulsed electron beam ablation*, *Science and Technology of Thin Film* (Singapore: World Scientific) **89**, 1995
- [22] S. D. Kovaleski, R.M. Gilgenbach, L.K. Ang, Y.T. Lau, *J. Appl. Phys.* **86**, 7129 (1999).
- [23] H.M. Christen, D. F. Lee, F.A. List, S.W. Cook, K.J. Leonard, L. Heatherly, P.M. Martin, M. Paranthaman, A. Goyal, C.M. Rouleau, *Supercond. Sci. Technol.* **18**, 1168 (2005).
- [24] V. A. Dediu, J. Lopez, F.C. Maticotta, P. Nozar, G. Ruani, R. Zamboni, C. Taliani, *Phys. Status Solidi B* **215**, 625 (1999).
- [25] R.J. Choudhary, S.B. Ogale, S.R. Shinde, V.N. Ulkarni, T. Venkatesan, K.S. Harshavardhan, M. Strikovski, B. Hannover, *Appl. Phys. Lett.* **84**, 1483 (2004).
- [26] M. Nistor, F. Gherendi, M. Magureanu, N.B. Mandache, A. Iochim, M. G. Banciu, L. Nedelcu, M. Popescu, F. Sava, H.V. Alexandru, *Appl. Surf. Sci.* **247**, 169 (2005).
- [27] H.L. Porter, C. Mion, A.L. Cai, X. Zhang, J.F. Muth, *Materials Science and Engineering B* **119**, 210-212 (2005).
- [28] P. Stadelmann: *JEMS Java Electron Microscopy software*, (2004), <http://cimewww.epfl.ch/>.
- [29] P. Shuk, H.D. Wiemhöfer, U. Guth, W. Göpel, M. Greenblatt, *Solid State Ionics* **89**, 179-196 (1996).
- [30] H.A. Harwig, A.G. Gerards, *J. Solid State Chem.* **26** 265 (1978).
- [31] G. Sakai, T. Jinkawa, N. Miura, N. Yamazoe, *Selective Detection of Nitrogen Monoxide by Using Bismuth Oxide-Based Sensor*, *Transducers'99*, Sendai, Japan, 7-10 pp. 146-149, June 1999.
- [32] A.Z. Adamyian, Z.N. Adamian, V.M. Aroutiounian, *Sens. Actuators B*, **93**, 416-421 (2003).
- [33] T. Takahashi, T. Esaka, H. Iwahara, *Journal of Applied Electrochemistry*, **7**, 299-302 (1977).
- [34] C.L. Gomez, O. Depablos-Rivera, J.C. Medina, P. Silva-Bermudez, S. Muhl, A. Zeinert, S.E. Rodil, *Solid State Ionics* **255**, 147-152 (2014).
- [35] S. Kac, T. Moskalewicz, *Inżynieria Materiałowa* **4**, 295-298 (2013).
- [36] J. Wu, C. Leighton, *Physical Review B* **67**, 174408-174408-16 (2003).
- [37] X. Yang, D.W. Park, M.I.I. Kim, *Korea J. Chem. Eng.* **24**, (4) 592-595 (2007).
- [38] P.R.N. Silva, A.B. Soares, *Ecletica Química* **34**, 31-38 (2009).
- [39] Y. Xiao Mao, *Applied Mechanics and Materials* **55-57**, 1957-1961 (2011).

- [40] Y.J. Yoo, K.K. Yu, Y.P. Lee, J.Y. Kim, Ch.J. Yu, K.W. Kim, J. Korean Physical Society **49**, 2397-2401 (2006).
- [41] K.H. Wong, W.Wu, P.W. Chan, J.T.Cheung, Thin Solid Films **312**, 7-10 (1998).
- [42] K.S. Hwang, H.M. Lee, S.S Min B.O Kang, J. of Sol-Gel Scien. and Tech. **18**, 175-180 (2000).
- [43] J. Szalc, A. Kopia, Ł. Cieniek, Thin films based on perovskite LaCoO<sub>3</sub> deposited by pulsed laser deposition, Inżynieria Materiałowa **6**, 903-906 (2013).
- [44] M. Chmielowska, S. Villain, A. Kopia, J.P. Dallas, J. Kusinski, J.R. Gavarrı, Ch. Leroux, Thin Solid Films **516**, 3747-3754 (2008).
- [45] S. Sun, L. Yang, G. Pang, S. Feng, Applied Catalysis A: General **401**, 199-203 (2011)
- [46] M. Lv, X. Xiu, Z. Pang, Y. Dai, L. Ye, Ch. Cheng, Sh. Han, Thin Solid Films **516**, 2017-2021 (2008).
- [47] M. Kumar, S. Srikanth, B. Ravikumar, T.C. Alex, S.K. Das, Materials Chemistry and Physics **113**, 803-815 (2009).
- [48] H.U. Krebs, M. Stoermer, S. Fehler, O. Bremert, M. Hamp, A. Pundt, H. Teichler, W. Blum, T.H. Metzger, Appl. Surf. Sc. **109/110**, 563 (1997).
- [49] A. Radziszewska, Journal of Microscopy **237**, 384-387 (2010).
- [50] A. Radziszewska, Solid State Phenomena **186**, 160-163 (2012).

*Received: 20 April 2015.*